REDUCED TRANSPORT AND E_R SHEARING IN IMPROVED CONFINEMENT REGIMES IN JT-60U

H. SHIRAI, M. KIKUCHI, T. TAKIZUKA, T. FUJITA, Y. KOIDE, G. REWOLDT
D. MIKKELSEN[1], R. BUDNY[1], W.M. TANG[1], Y. KISHIMOTO, Y. KAMADA
T. OIKAWA, O. NAITO, T. FUKUDA, N. ISEI, Y. KAWANO, M. AZUMI
and the JT-60 TEAM
Japan Atomic Energy Research Institute
Naka-machi, Naka-gun, Ibaraki-ken, 311-0193 Japan
[1]Princeton Plasma Physics Laboratory, Princeton, New Jersey, 08543 USA

Abstract

The global confinement and the local transport properties of improved core confinement plasmas in JT-60U have been studied in connection with E_r shear formation. The improved core confinement mode with ITB, the internal transport barrier, is roughly classified into "parabolic" type ITBs and "box" type ITBs. The parabolic type ITB has the reduced thermal diffusivity, χ, in the core region; however, the E_r shear, dE_r/dr, is not so strong. The box type ITB has a very strong E_r shear at the thin ITB layer and the χ value decreases to the level of neoclassical transport there. The estimated $E\times B$ shearing rate, $\omega_{E\times B}$, becomes almost the same as the linear growth rate of the drift microinstability, γ_L, at the ITB layer in the box type ITB. Experiments of hot ion mode plasmas during the repetitive L-H-L transition shows that the thermal diffusivity clearly depends on the E_r shear and the strong E_r shear contributes to the reduced thermal diffusivity.

1. INTRODUCTION

Various kinds of improved core confinement (ICC) plasmas such as hot ion H-mode plasmas [1], high β_p H-mode plasmas [2], and reversed shear plasmas [3] have been found in JT-60 with large fusion triple product, $n_D(0)\tau_E T_i(0)$, and high equivalent D-T fusion amplification factor, Q_{DT}^{eq} [4]. In this paper, the improved energy confinement and the reduced thermal transport in such ICC plasmas are investigated in connection with the formation of a sheared radial electric field, E_r.

These ICC plasmas have much larger stored energy in the core region compared with L-mode plasmas, and are often accompanied by an internal transport barrier (ITB), which is formed at a location r=$r_{\rm ITB}$ inside the plasma. The pressure gradient changes discontinuously at r=$r_{\rm ITB}$. Figure 1 shows typical profiles of the electron temperature (solid line and closed circles), T_e, the ion temperature (broken line and the open circles), T_i, and the electron density (dotted line and closed squares), n_e, in (a) a normal shear plasma and (b), (c) reversed shear plasmas with ITBs.

Hereafter, we call the ITB of (a) and (b) the "parabolic type" ITB, in which the pressure gradient is larger over the core region r<$r_{\rm ITB}$ than that of peripheral region in r>$r_{\rm ITB}$. The T_i profile shows the parabolic type ITB easier than n_e or T_e profiles. The discontinuous change at r=$r_{\rm ITB}$ is observed only in T_i gradient for case (a) and in n_e, T_e, T_i gradient for case (b). In JT-60U, the parabolic type ITB could be observed in any kind of improved confinement mode, the hot ion H-mode, the high β_p H-mode and the reversed shear plasmas.

We call the ITB of (c) the "box type" ITB. Within the ITB layer around r=$r_{\rm ITB}$, the pressure gradient is remarkably large. At both boundaries of the ITB layer, the pressure gradient

discontinuously change. The box type ITB is observed in n_e, T_e, T_i gradient for case (c). Since the T_i profile shows the box type ITB easier than n_e or T_e profiles, the combination of the box type ITB in T_i profile and the parabolic type ITBs in n_e and T_e profiles is observed. The box type ITB was observed only in reversed shear plasmas so far.

2. METHOD OF ANALYSIS

The transport and the confinement properties of JT-60U plasmas are estimated by the 1.5 dimensional (2 dimensional equilibrium and 1 dimensional transport) transport analysis code, TOPICS [5], and the orbit following Monte-Carlo code, OFMC [6]. The OFMC code considers the ripple loss, the orbit loss and the charge exchange loss of the fast ions generated by NBI and estimates the density profile and the pressure profile of the fast ions, the profile of the NBI particle source and the energy deposition profiles to electrons and thermal ions. The TOPICS code uses the results of the OFMC code and calculates the profiles of thermal diffusivity, χ, and the radial electric field, E_r.

The E_r profile is calculated as follows. The momentum balance and the heat momentum balance equations parallel to the magnetic field give the equation of flux averaged parallel flow [7],

$$\left\langle B u_{\|I} \right\rangle = \sum_{j=1}^{7} \left\{ \left[\left(\widehat{L} - \widehat{M} \right)^{-1} \widehat{M} \right]_{I,j} V_j - \left[\left(\widehat{L} - \widehat{M} \right)^{-1} \right]_{I,j} S_j - e_j n_j \left[\left(\widehat{L} - \widehat{M} \right)^{-1} \right]_{I,j} \langle \boldsymbol{B} \cdot \boldsymbol{E} \rangle \right\} \tag{1}$$

Here, $\widehat{L}$, $\widehat{M}$, V_j and S_j are the normalized friction matrix, the normalized viscosity matrix, the thermodynamic force vector, the momentum and the heat momentum source vectors, respectively [8]. The suffix "I" denotes the variables related to the impurity. The terms with suffix j=1$\sim$4 denote the momentum of electrons, ions, impurities and fast ions, respectively. The terms with suffix j=5$\sim$7 denote the heat momentum of electrons, ions and impurities, respectively. The term V_j (j=1$\sim$4) includes $d\Phi/d\psi$. In the following analyses, the second and the third terms of the RHS of eq.(1) are neglected. The neglect of the second term is valid for the case of almost balanced NBI injection.

The toroidal rotation of the impurity is expressed by the impurity flow parallel and perpendicular to the magnetic field [9],

$$u_{I\phi} = \frac{B_\phi}{\langle B^2 \rangle} \left\langle B u_{\|I} \right\rangle - \left(1 - \frac{B_\phi^2}{\langle B^2 \rangle} \right) R \left(\frac{d\Phi}{d\psi} + \frac{1}{e_I n_I} \frac{dP_I}{d\psi} \right) \tag{2}$$

By eliminating the term $\left\langle B u_{\|I} \right\rangle$ from eqs.(1) and (2) and using the toroidal velocity profile of the impurity, $u_{I\phi}$, measured by charge exchange recombination spectroscopy (CXRS), the E_r profile is estimated as

$$E_r = -\frac{d\Phi}{d\rho} = \frac{1}{\sum_{j=1}^{4} \alpha^*_{I,j}} \left(-\frac{\langle B^2 \rangle}{(RB_\phi)^2} \frac{d\psi}{d\rho} R u_{I\phi} - \sum_{j=1}^{4} \alpha^*_{I,j} \frac{1}{e_j n_j} \frac{dP_j}{d\rho} + \sum_{j=1}^{3} \alpha^*_{I,j+4} \frac{1}{e_j} \frac{dT_j}{d\rho} \right) \tag{3}$$

Here, $\alpha^*_{I,j} = \alpha_{I,j} + \left(\langle B^2 \rangle / B_\phi^2 - 1 \right) \delta_{I,j}$ and the coefficient $\alpha_{i,j}$ is an element of $\left(\widehat{L} - \widehat{M} \right)^{-1} \widehat{M}$.

The neoclassical thermal diffusivity was often estimated by Chang and Hinton's formula [10]. In this paper, the matrix inversion method (MI method) developed for the bootstrap current was applied to the estimation of the neoclassical ion thermal diffusivity [11 – 13]. The

neoclassical thermal diffusivity of species j, $\chi_j^{\rm NC}$, is made up of classical and Pfirsch-Schlüter (CPS) diffusion and Banana-Plateau (BP) diffusion as follows,

$$\chi_j^{\rm NC} = \sqrt{\varepsilon}\,\widehat{\rho}_{p\ j}^{2}\,\nu_{j,j}\left(\widehat{K}_{2\ j}^{\rm CPS}+\widehat{K}_{2\ j}^{\rm BP}\right) \tag{4}$$

$$\widehat{K}_{2\ j}^{\rm CPS} = \frac{B_0^2\left(\widehat{l}_{2,1}^{j,j}-\widehat{l}_{2,2}^{j,j}\right)}{2\sqrt{\varepsilon}\left\langle B^2\right\rangle}\left[\frac{\left\langle R^2\right\rangle\left\langle B^2\right\rangle}{\left(RB_\phi\right)^2}-1\right] \tag{5}$$

$$\widehat{K}_{2\ j}^{\rm BP} = \frac{B_0^2}{2\sqrt{\varepsilon}\left\langle B^2\right\rangle}\left[\widehat{\mu}_3^j\left(1-\alpha_{j+3,j}+\alpha_{j+3,j+3}\right)-\widehat{\mu}_2^j\left(1+\alpha_{j,j}-\alpha_{j,j+3}\right)\right] \tag{6}$$

Here, $\widehat{l}$ and $\widehat{\mu}$ are elements of the normalized friction matrix $\widehat{L}$ and normalized viscosity matrix $\widehat{M}$, respectively. The total ion neoclassical thermal diffusivity $\chi_{\rm ION}^{\rm NC}$ is obtained as $n_i/\left(n_i+n_I\right)\chi_i^{\rm NC}+n_I/\left(n_i+n_I\right)\chi_I^{\rm NC}$ on the condition of the same temperature for main ions and the impurities.

The linear growth rate of high-n toroidal drift modes was analyzed by a linear toroidal kinetic microinstability analysis code, the FULL code [14] under the collaboration with the Princeton Plasma Physics Laboratory. In the FULL code, the largest linear growth rate, γ_L, is calculated at some radius by changing the $k_\theta\rho_i$ value, where k_θ and ρ_i are the wave number in the poloidal direction and the ion Larmor radius, respectively.

In order to compare with γ_L, the $E\times B$ shearing rate, $\omega_{E\times B}$, is estimated as [15]

$$\omega_{E\times B}\equiv\frac{\left(RB_\theta\right)^2}{B}\frac{\partial}{\partial\psi}\left(\frac{E_r}{RB_\theta}\right) \quad . \tag{7}$$

3. GLOBAL ENERGY CONFINEMENT PROPERTY FOR r<$r_{\rm ITB}$

In this section, the energy confinement property in the core region of the parabolic type ITB and the box type ITB are compared. The ICC plasmas with I_p=1.5 MA, B_t=3.5~4.0 T, $\overline{n}_e$=2.0~3.7×10^{19} m^{-3} and P_{abs}=8~15 MW are investigated. Here the following variable for the incremental thermal stored energy in the region $r<r_{\rm ITB}$ is calculated by

$$\Delta W_{th}^{\rm in}=\frac{3}{2}k_B\int_0^{r_{\rm ITB}}\left[\left(n_e(r)T_e(r)+n_i^{th}(r)T_i(r)\right)-\left(n_e(r_{\rm ITB})T_e(r_{\rm ITB})+n_i^{th}(r_{\rm ITB})T_i(r_{\rm ITB})\right)\right]dV \tag{8}$$

based on the boundary density and temperature at r=$r_{\rm ITB}$. The value of $\Delta W_{th}^{\rm in}$ denotes the ability of each type of ITB to confine the stored energy in the core region. The plasma volume and heating power in the region $r<r_{\rm ITB}$ are $V^{\rm in}$ and $P^{\rm in}$, respectively. The dependence of the volume averaged values, $\Delta W_{th}^{\rm in}/V^{\rm in}$, on $P^{\rm in}/V^{\rm in}$ for (a) electrons and (b) ions is shown in Fig. 2. Open symbols and closed symbols denote the cases of the parabolic type ITB in T_i profile and the cases of the box type ITB in T_i profile, respectively. Circles and squares denote normal shear and reversed shear, respectively. The slope from the origin corresponds to the core energy confinement time. It is clear that the core energy confinement time of the box type ITB is twice as large as that of the parabolic type ITB.

The concentration of the absorbed power in the region surrounded by the ITB (r=$r_{\rm ITB}$), $P_{abs}^{\rm in}/P_{abs}^{\rm total}$, is estimated as a function of the relative core plasma volume, $V^{\rm in}/V^{\rm total}$. They are almost the same between the parabolic type ITB and the box type ITB. Therefore the better core confinement of the box type ITB cannot be ascribed to the intensive core heating.

4. SHEARED RADIAL ELECTRIC FIELD FORMATION AND REDUCTION OF LOCAL TRANSPORT

4.1. Steady State Case

The relation among the improved energy confinement, the reduction of thermal diffusivity, χ, and the sheared E_r is discussed in this section. First, plasmas in the steady state are analyzed. Figure 3 shows the profiles of the electron and ion thermal diffusivities, χ_e (thin solid line) and χ_i (broken line), the neoclassical $\chi^{\rm NC}$ (dotted line) and the radial electric field, E_r (thick solid line). Each part of this figure corresponds to that of Fig. 1.

The $\chi^{\rm NC}$ was estimated by the matrix inversion (MI) method [11]. The $\chi^{\rm NC}$ value estimated by the MI method is about half of that estimated by the Chang-Hinton formula [10] in the parameter region represented by Fig. 1. Since the collision frequencies of electrons and ions are in the banana regime, the orbit squeezing effect is taken into account in the calculation of $\chi^{\rm NC}$. However, the difference in $\chi^{\rm NC}$ between results with and without the orbit squeezing effect is small. Only within the ITB layer of the box type ITB, 40% reduction of $\chi^{\rm NC}$ is obtained.

In the case of a parabolic type ITB, the thermal diffusivity in the region $r<r_{\rm ITB}$ is remarkably smaller than that in the region $r>r_{\rm ITB}$. The value of χ_i decreases to the level of $\chi^{\rm NC}$ near the magnetic axis. The characteristic of improved core confinement in the parabolic type ITB is shown by the reduction of thermal diffusivity over the whole area of the core plasma, which is the well-accepted point of view. A negative E_r shear ($dE_r/dr<0$) is obtained in the region $r<r_{\rm ITB}$. However, the E_r shear is not so strong compared with that in the ITB layer of the box type ITB.

In the case of a box type ITB, on the other hand, χ_e and χ_i at the ITB layer are quite small; their values are reduced to the level of $\chi^{\rm NC}$, whereas the value of the thermal diffusivity in the core region $r<r_{\rm ITB}$ is not always small. The characteristics of improved core confinement with a box type ITB are different from those of a parabolic type ITB. Good confinement is not directly related to the reduced thermal diffusivity overall of the core region. A stronger barrier against the outward heat flow is formed at the thin ITB layer and the heat flow is dammed up at the ITB in the region $r<r_{\rm ITB}$. In the vicinity of the ITB layer where χ_e and χ_i become quite small, a strong E_r shear layer is localized. In this region, the contributions of the toroidal rotation and the pressure gradient to E_r, that is the first and the second terms of the RHS of eq.(3), are of the same order of magnitude.

4.2. Repetitive L-H-L Transition Case

In this subsection, the relation between the local transport and the sheared E_r is analyzed during the dynamic change of energy confinement. A hot ion mode plasma with I_p=2.5 MA, B_t=4.2 T and $T_i(0)$>20 keV is investigated. Figure 4 shows the time evolution of the NBI injection power, P_{NBI}, the diamagnetic stored energy, W_{dia}, the line averaged electron density, $\overline{n}_e$, the T_e and T_i at the half minor radius and the intensity of the D_α signal of this plasma. The L-phase and H-phase confinement appear repetitively. In this plasma, the T_i profile is fairly peaked, but no clear ITB was observed.

In Fig. 5, the profiles of χ_e, χ_i and E_r in the (a) H-phase and (b) L-phase are shown. At the L-H and H-L transitions, the shear in the toroidal rotation changed instantaneously within the time resolution of the CXRS measurement. The E_r shear becomes strong in the H-phase and weak in the L-phase overall of the plasma region. At the same time, both χ_e and χ_i in the H-phase become about half of those in the L-phase.

The plasma parameter profiles at a selected time during the H-phase (reduced χ) and the

L-phase (enhanced χ) become almost the same, because the plasma changes repetitively. This suggests a conclusion that the thermal diffusivity clearly depends on the E_r shear and the strong E_r shear contributes to the reduced thermal diffusivity.

4.3. Linear Growth Rate of Microinstabilities and E×B Shearing Rate

The box type ITB has a very large pressure gradient at the thin ITB layer, which may become a free energy source to excite microinstabilities. At the same time, strong E_r shear is formed at the ITB layer, which induces a sheared $E\times B$ flow in the poloidal direction and suppresses microinstability [15].

Figure 6 shows the profiles of T_e, T_i, n_e, γ_L and $\omega_{E\times B}$, in the peaked pressure profile high β_p plasma ((a) and (b)) with I_p=1.5 MA and B_t=3.5 T and the box type ITB reversed shear plasma ((c) and (d)) with I_p=1.2 MA and B_t=3.5 T. The profile of γ_L is calculated by the FULL code for the electrostatic toroidal drift mode (trapped-electron-ITG mode). In the former case, γ_L is much larger than $\omega_{E\times B}$ except near the magnetic axis. The $E\times B$ sheared flow is not strong enough to suppress the microinstability. This is consistent with the fact that χ_i is larger than $\chi^{\rm NC}$ except for the region near the magnetic axis. In the latter case, the ITB layer is formed in the region $0.4<r/a<0.6$. Within the ITB layer, $\omega_{E\times B}$ becomes almost as large as γ_L. It is expected that the microinstability in the ITB layer is suppressed and favorable energy confinement is realized.

5. TOROIDAL ROTATION SHEAR AND CONFINEMENT

The relation of E_r shear to the reduced transport and the improved confinement has been presented in the previous sections. The E_r shear depends on the toroidal rotation shear and the shear of the pressure gradient. In this section, the effect of toroidal rotation shear on the energy confinement is studied.

JT-60U has two units of co tangential NBI and two units of counter tangential NBI. The co-rotating plasmas and the counter-rotating plasmas are obtained by selecting these tangential NBI units. A set of ELMy H-mode discharges with I_p=1.0 MA, B_t=2.1 T, $\overline{n}_e$=1.9$\sim$2.1$\times10^{19}$m^{-3}, P_{abs}=4.4$\sim$6.3 MW and $T_i(0)$=4$\sim$5 keV was carried out. The plasmas are not in the core improved confinement mode because of the small NBI power.

Figure 7 shows the profiles of (a) V_t, (b) n_e and (c) T_i for the co-rotating plasma (closed circles, with two units of co-tangential NBI), the almost no rotating plasma (closed squares, with one co- and one counter-tangential NBI) and the counter-rotating plasma (open circles, with two units of counter-tangential NBI). In addition to the tangential NBI units, the perpendicularly injected NBI units are used. The total absorbed power is 6.0 MW for all cases. The values of the total injected NBI power are 8.0 MW, 8.8 MW and 10.0 MW for the co-rotating plasma, the almost no rotating plasma and the counter-rotating plasma, respectively. The ratio of orbit loss and ripple loss of fast ions is larger for the counter NBI injected (counter-rotating) plasma.

The toroidal rotation shear for each case is almost constant overall of the plasma. The co-rotating plasma has slightly higher density compared with the counter-rotating plasma, in spite of having almost the same temperature profile. The profile of the absorbed power density is almost the same for each case except in the central region $r/a<1/3$ as shown in Fig. 8.

The HH-factor for the thermal energy confinement time based on the ITER97H-ELMy scaling law [16],

$$\tau_{th}^{\rm ELMy}({\rm s}) = 0.029\, I_p^{0.90}({\rm MA})\, B_t^{0.20}({\rm T})\, P_{abs}^{-0.66}({\rm MW})\, n_e^{0.40}(10^{19}{\rm m}^{-3})\, M_i^{0.2}\, R^{1.84}({\rm m})\, a^{0.19}({\rm m})\, \kappa^{0.92}\ , \quad (9)$$

is shown in Fig. 9. It is clear that the co-rotating plasma has a higher HH-factor than the counter-rotating plasma. In order to clarify the difference in energy confinement from the view point of E_r shear, it is necessary to evaluate the second term (momentum source term) in the RHS of eq.(3), because the momentum injection by the parallel NBI is essentially important for these experiments. We are going to evaluate the momentum source profile by modifying the OFMC code. The comprehensive study of the confinement with the E_r shear for ELMy H-mode plasmas will be done in the near future.

6. CONCLUSION

The global confinement and the local transport properties of improved core confinement plasmas in JT-60U have been studied in connection with radial electric field shear formation. The improved core confinement mode with ITBs is roughly classified into "parabolic" type ITBs and "box" type ITBs. The parabolic type ITB shows a reduction of the thermal diffusivity, χ, overall of the core region surrounded by $r{=}r_{\rm ITB}$; however, the E_r shear, dE_r/dr, in the core region of a parabolic type ITB is not so strong. The E_r shear in the box type ITB is very strong only at the thin ITB layer and the χ value decreases to the level of neoclassical transport there. Experiments of hot ion mode plasmas during the repetitive L-H-L transition shows that the thermal diffusivity clearly depends on the E_r shear and the strong E_r shear contributes to the reduced thermal diffusivity. The energy confinement property of box type ITBs in the core region surrounded by $r{=}r_{\rm ITB}$ is about twice as large as that of parabolic type ITBs.

The estimated $E{\times}B$ shearing rate, $\omega_{E\times B}$, is much smaller than the linear growth rate of the microinstability, γ_L, for the parabolic type ITB. For the box type ITB, on the other hand, the $\omega_{E\times B}$ value is almost the same as γ_L at the ITB layer. A series of ELMy H-mode experiments with different plasma rotation showed that the co-rotating plasma is more favorable for energy confinement than the counter-rotating plasma in the non-ICC ELMy H-mode plasmas.

References

[1] KIKUCHI, M., SHIRAI, H., et al., in *Proc. 14th Int. Conf. on Plasma Phys. and Controlled Nucl. Fusion Res.*, Würzburg, 1992 (IAEA, Vienna, 1993), Vol.1, p.189.

[2] KOIDE, Y., ISHIDA., S., KIKUCHI., M., et al., in *Proc. 15th Int. Conf. on Plasma Phys. and Controlled Nucl. Fusion Res.*, Seville, 1994 (IAEA, Vienna, 1995), Vol.1, p.199.

[3] FUJITA, T., IDE, S., SHIRAI, H., KIKUCHI, M., et al., Phys. Rev. Lett., **78** (1997) 2377.

[4] TOBITA, K. AND THE JT-60 TEAM, in *Proc. 25th Eur. Conf. on Controlled Fusion and Plasma Physics*, Prague, 1998, to be published in Plasma Physics and Controlled Fusion.

[5] SHIRAI, H., TAKIZUKA, T., NAITO, O., et al., J. Phys. Soc. Jpn., **64** (1995) 4209.

[6] TANI, K., AZUMI, M., KISHIMOTO, H., J. Phys. Soc. Jpn., **50** (1981) 1726.

[7] KIKUCHI, M., AZUMI, M., Plasma Phys. Control. Fusion, **37** (1995) 1215.

[8] HIRSHMAN, S.P., SIGMAR, D.J., Nucl. Fusion, **21** (1981) 1079.

[9] HIRSHMAN, S.P., Phys. Fluids, **19** (1976) 155.

[10] CHANG, C.S., HINTON, F.L., Phys. Fluids, **29** (1986) 3314.

[11] KIKUCHI, M., SHIRAI, H., et al., JAERI Research 98-039 (1998) p.43.

[12] KIKUCHI, M., AZUMI, M., TSUJI, et al., Nucl. Fusion, **30** (1990) 343.

[13] TANI, K., AZUMI, M., DEVOTO, R.S., J. Comp. Phys., **98** (1992) 332.

[14] REWOLDT, G., TANG, W.M., CHANCE, M.S., Phys. Fluids, **25** (1982) 480.

[15] HAHM, T.S, BURRELL, K.H., Plasma Phys. Controlled Fusion, **38** (1996) 1667.

[16] ITER CONFINEMENT DATABASE AND MODELLING WORKING GROUP (presented by J. G. Cordey), Plasma Phys. Controlled Fusion, **39** (1997) B115.

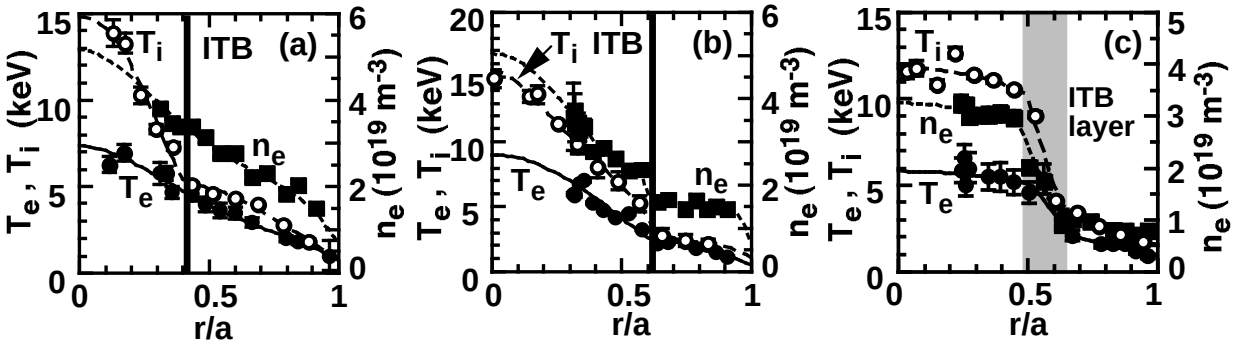

Fig. 1 Profiles of T_e (solid line), T_i (broken line) and n_e (dotted line) of ICC plasmas with (a) normal shear, parabolic type ITB, (b) reversed shear, parabolic type ITB, (c) reversed shear, box type ITB for I_p=1.5 MA and B_t=3.5~4.0 T.

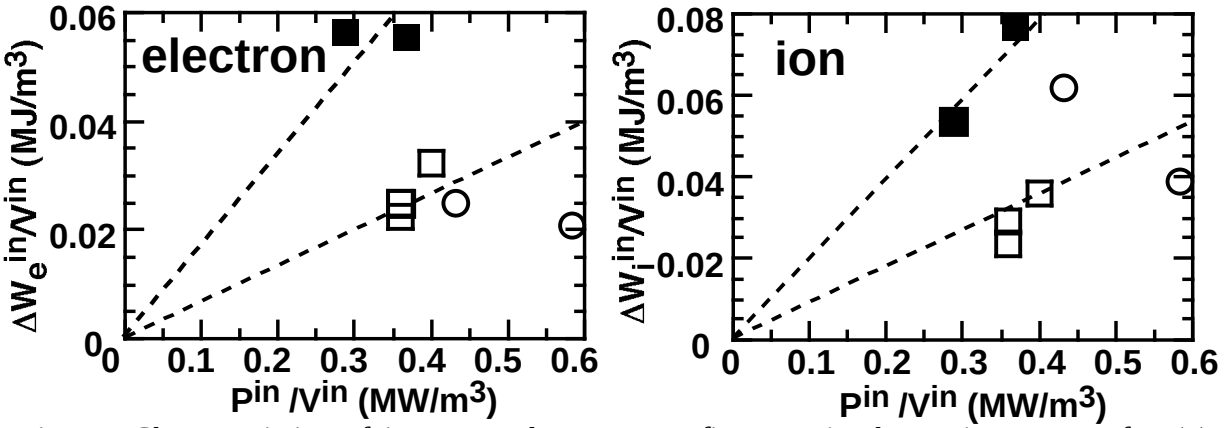

Fig. 2 Characteristics of incremental energy confinement in the region $r<r_{ITB}$ for (a) electrons and (b) ions for I_p=1.5 MA and B_t=3.5~4.0 T. Open symbols and closed symbols denote the parabolic type ITB and the box type ITB, respectively. Circles and squares denote the normal shear and reversed shear, respectively.

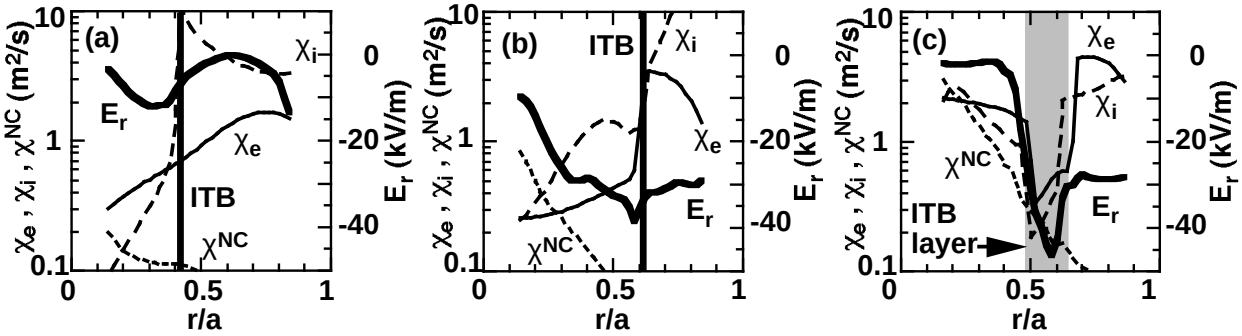

Fig. 3 Profiles of χ_e (thin solid line), χ_i (broken line), χ_{NC} (dotted line) and E_r (thick solid line). Each part of this figure corresponds to that of Fig. 1.

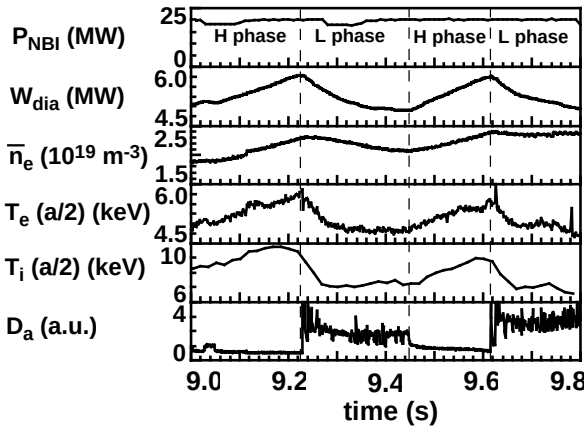

Fig. 4 Time evolution of NBI injection power, P_{NBI}, diamagnetic stored energy, W_{dia}, line averaged electron density, $\overline{n}_e$, T_e (a/2), T_i (a/2) and D_α intensity in hot ion plasma (I_p=2.5 MA and B_t= 4.0 T) during repetitive L-H-L transition phase.

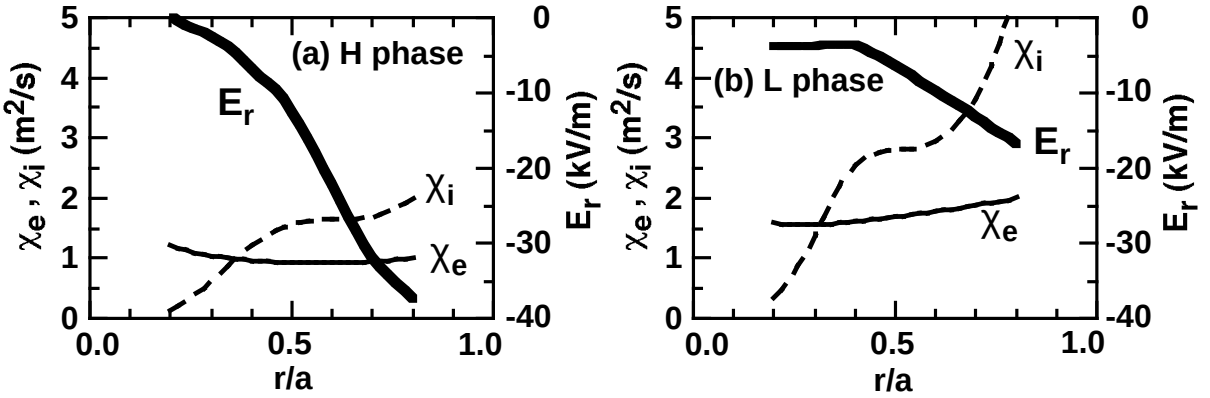

Fig. 5 Profiles of χ_e (thin solid line), χ_i (broken line) and E_r (thick solid line) for (a) H phase and (b) L phase.

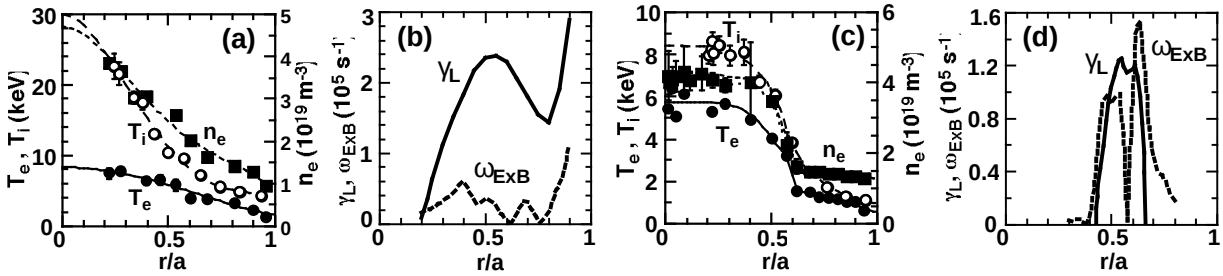

Fig. 6 Profiles of T_e (solid line), T_i (broken line) n_e (dotted line), growth rate of the microinstability, γ_L, (solid line) and ExB shearing rate, ω_{ExB}, (dotted line) in normal shear hot ion plasma ((a) and (b)) and in reversed shear plasma ((c) and (d)).

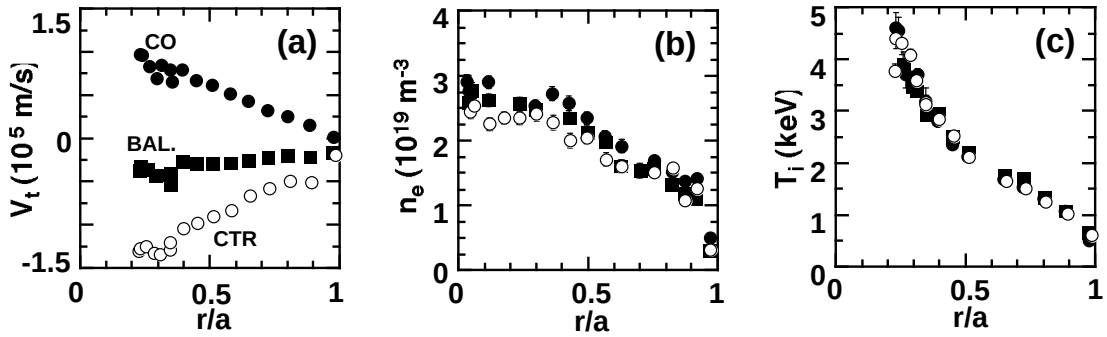

Fig. 7 Profiles of (a) V_t , (b) n_e and (c) T_i in co-rotating plasma (closed circles), nearly no rotating plasmas (closed squares) and counter-rotating plasma (open circles) for ELMy H-mode phase.

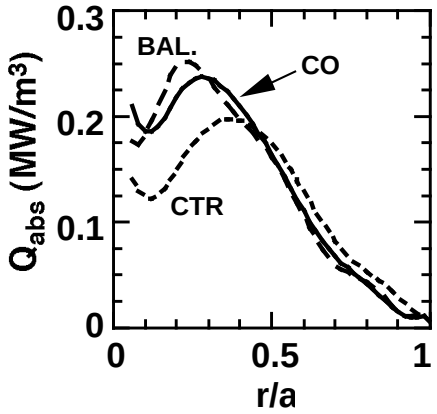

Fig. 8 Profiles of absorbed power.

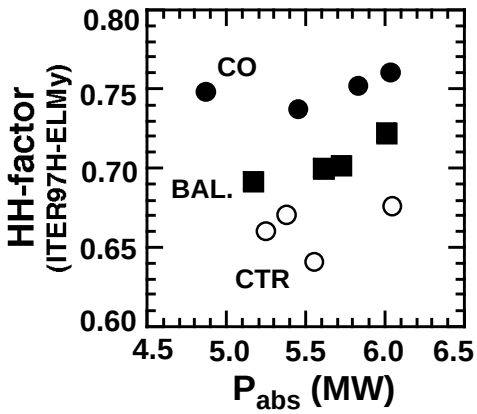

Fig. 9 Dependence of HH-factor on absorbed power.